https://doi.org/10.1038/s44400-026-00093-9

# Coronary artery calcification reflects cognitive and cerebrovascular alterations in cognitively unimpaired adults



Sofia Marcolini[1,2] ✉, Jaime D. Mondragón[1,2,3,4], Johannes Castelein[5,6,7], Thomas W. Okell[8], Charlotte E. Teunissen[9], Inge M. W. Verberk[9], Anouk van der Hoorn[7], Rozemarijn Vliegenthart[7], Rudi A. J. O. Dierckx[10], Ronald J. H. Borra[6,7,10,11] & Peter P. De Deyn[1,12]

Coronary artery calcification (CAC) entails arterial wall hardening and lipid-rich plaque accumulation and may contribute to early cognitive decline. Its association with cognition, brain structure and function, Alzheimer's disease, neurodegeneration, and inflammatory and lipid biomarkers remains unclear. We conducted a cross-sectional study of 278 cognitively unimpaired adults aged ≥ 50 years with absent (score = 0; $n = 151$) or high CAC (score ≥ 300; $n = 127$). Participants underwent cognitive testing, serum assays (Aβ42/40, pTau181, NfL, GFAP, inflammatory and lipid markers), and multimodal MRI (structural, resting-state and vessel encoded arterial spin labeling). High CAC was associated with lower general cognition, increased white matter hyperintensities, altered hippocampal and sensorimotor connectivity, and reduced perfusion in the inferior frontal gyrus pars opercularis. No group differences emerged in the serum biomarkers. These results reveal that high CAC is associated with cognitive and cerebrovascular changes independent of Alzheimer's disease biomarker increase, suggesting vascular pathways in early brain aging.

Coronary artery calcification is characterized by arterial wall hardening and accumulation of lipid-rich plaques, beginning as early as the second or third decade of life[1]. It can negatively impact brain health through pathways involving cerebrovascular structural and functional disruption[2,3] and is associated with increased risk of cardiovascular events[4], mortality[5,4], and dementia[6–9]. It is measurable via non-invasive coronary artery calcium scoring from cardiac computed tomography[10], with a score higher than 300 being indicative of more extensive disease[11]. Coronary artery calcification may be a relevant measure to indicate vulnerability for cognitive decline, although a comprehensive assessment of how it affects measures related to cognitive decline is lacking.

The impact of coronary calcification on cognition remains poorly understood, and evidence on its relationship with specific cognitive domains is inconsistent. Some studies report links to executive function and processing speed[12,13], others to memory[13,14], while some observe no significant associations[15]. Several biological mechanisms may underlie the connection between coronary calcification and cognitive decline, including reduced cardiac output due to coronary artery narrowing, impaired autoregulation of cerebral blood flow, increased pulsatility damaging small vessels, and systemic inflammation contributing to neurovascular dysfunction[2,3].

Whether these mechanisms linked to coronary calcification lead to brain changes can be explored with neuroimaging. Regarding structural brain changes, previous studies have reported associations between coronary calcification and cortical thinning[16] as well as a marker of small vessel disease[17,18], though most rely on categorical imaging ratings rather than quantitative assessments[19,20]. Concerning functional brain changes, the

[1]Department of Neurology, University Medical Center Groningen, University of Groningen, Groningen, The Netherlands. [2]The Research School of Behavioural and Cognitive Neurosciences, University of Groningen, Groningen, The Netherlands. [3]Laboratorio de Psicofisiología, Departamento de Neurobiología Conductual y Cognitiva, Instituto de Neurobiología, Universidad Nacional Autónoma de México, Querétaro, Mexico. [4]Life-Span Human Senses Lab,Department of Psychology, San Diego State University, San Diego, CA, USA. [5]Department of Biomedical Sciences, Faculty of Health and Medical Sciences, University of Copenhagen, Copenhagen, Denmark. [6]Department of Radiology, Medical University of Gdańsk, Gdańsk, Poland. [7]Department of Radiology, University Medical Center Groningen, University of Groningen, Groningen, The Netherlands. [8]Oxford Centre for Integrative Neuroimaging, FMRIB, Nuffield Department of Clinical Neurosciences, University of Oxford, Oxford, United Kingdom. [9]Neurochemistry Laboratory, Department of Laboratory Medicine, Amsterdam University Medical Centers, Vrije Universiteit Amsterdam, Amsterdam Neuroscience, Amsterdam, The Netherlands. [10]Department of Nuclear Medicine and Molecular Imaging, University Medical Center Groningen, University of Groningen, Groningen, The Netherlands. [11]Department of Radiology, Turku University Hospital, Turku, Finland. [12]Neurochemistry and Behaviour group, Experimental Neurobiology Unit, Department of Biomedical Sciences, University of Antwerp, Antwerp, Belgium.
✉e-mail: s.marcolini@umcg.nl

**Table 1 | Sample characteristics**

| Characteristic | Total $n = 278$ | CAC = 0 $n = 151$ | CAC ≥ 300 $n = 127$ | *p*-value |
|---|---|---|---|---|
| Sex (Female) | 114 (41%) | 82 (54%) | 32 (25%) | <0.001 |
| Education (Years) | 13.6 (3.8) | 13.8 (3.7) | 13.4 (3.9) | 0.20 |
| Age (Years) | 68 (9) | 67 (8) | 70 (9) | 0.02* |
| Self-reported ancestry | | | | 0.90 |
| Northern/Western European | 277 (100%) | 150 (99%) | 127 (100%) | |
| Middle Eastern/North African | 1 (0.4%) | 1 (0.7%) | 0 (0%) | |
| Current smoking (Yes) | 20 (7.2%) | 6 (4.0%) | 14 (11%) | 0.02* |
| Glasses of alcohol per week | 2 (1) | 2 (1) | 2 (1) | 0.08 |
| Years Memolife-Imalife[a] | 2.59 (1.14) | 2.56 (1.15) | 2.62 (1.13) | 0.50 |
| Missing | 2 | 0 | 2 | |
| MMSE total | 29 (1) | 29 (1) | 29 (1) | 0.30 |
| CAC score | 395 (619) | 0 (0) | 864 (658) | <0.001* |

*CAC* coronary artery calcium, *MMSE* mini mental state examination.

*$p$-value < 0.05.

[a]indicates the years between the CT scan and the neuropsychological and blood assessments.

relationship between coronary calcification and brain functional connectivity and cerebral blood flow is still unexplored. Although functional brain connectivity, which captures synchronized neural activity across brain regions, was found to be disrupted in individuals with coronary artery disease[21,22] and in those with elevated cardiovascular risk despite preserved cognition[23].

In parallel, it is unclear whether coronary calcification is associated with neurodegeneration or Alzheimer's-specific pathology. Biomarkers of amyloid, tau, and neurodegeneration (ATN) begin to change decades before the onset of clinical symptoms[24]. In cognitively unimpaired individuals, ATN biomarkers can identify individuals at heightened risk of future decline[25,26]. Recently developed blood-based biomarkers, including plasma phosphorylated tau isoforms, amyloid-β42/40 ratio, glial fibrillary acidic protein (GFAP), and neurofilament light chain (NfL), offer practical and scalable alternatives to cerebrospinal fluid and PET imaging, with high diagnostic validity[27,28].

Additionally, at the basis of coronary calcification are atherosclerotic processes, which are largely driven by inflammation[1,3]. In atherosclerosis, inflammatory cytokines are critical to disease initiation and plaque progression. Similarly, the inflammatory hypothesis of Alzheimer's disease posits that neuroinflammation is a pathogenic factor in the early stages and progression of the disease, rather than a mere consequence of neurodegeneration[29,30]. Findings on the associations between systemic markers of inflammation and coronary calcification are conflicting, with some finding associations[31,32] and others showing only weak or inconsistent results[33,34].

To investigate whether coronary calcification is associated with measures of cognitive decline, we investigated whether cognitively unimpaired adults with absent or high levels of coronary calcification differed cross-sectionally in cognitive performance, structural brain volumes, brain functional connectivity, cerebral blood flow, blood-based Alzheimer's disease, neurodegeneration, inflammatory, and lipid biomarkers. We hypothesized that, in a cross-sectional comparison, individuals with high coronary calcification would demonstrate poorer outcomes relative to those without calcification. Our aim is ultimately to elucidate the early vascular and cerebrovascular mechanisms that may contribute to cognitive decline in aging individuals.

## Results

### Sample characteristics

Of the 397 participants contacted through the Imalife study, 285 gave informed consent to participate in this study. 278 cognitively unimpaired older adults were finally included in the study: 151 with a coronary artery calcium (CAC) score of 0 (absent CAC; 67 ± 8 years old; 54% females) and 127 with a CAC score ≥ 300 (high CAC; 70 ± 9 years old; 25% females). Individuals in the high CAC group were older, more often male, and more likely to be current smokers compared to those with absent CAC (Table 1).

### Cognitive measures and manual dexterity

General cognition was significantly lower in participants with high CAC compared to those with absent CAC (adjusted mean difference = 0.28; 95% CI: −0.48 to −0.08), after correction for multiple comparisons and demographic covariates. No significant between-group differences were observed in memory, executive function, information processing, or manual dexterity after correction for multiple comparisons and demographic covariates (Table 2).

### Serum biomarkers and brain volumes

All serum biomarker concentrations were well above the limits of quantification for the respective assays, ensuring measurement validity. No group differences were observed in serum Alzheimer's disease biomarkers (Aβ42/Aβ40 ratio, pTau181, GFAP, NfL), inflammatory markers (CRP, IL-1β, IL-6, TNF-α), or lipid measures (HDL, LDL, triglycerides, glucose) following multiple comparison correction between absent and high CAC groups.

Compared to previously obtained NfL reference ranges for controls (accessible at: https://mybiomarkers.shinyapps.io/Neurofilament/), the values found in our study seem to overall be higher, specifically belonging to the control 75th–90th percentile (see Supplementary Tables 1 and 2). Trends toward elevated non fasting glucose and IL-6 levels in the high CAC group were shown (Table 3).

Participants with high CAC exhibited lower total brain volume (adjusted mean difference = 6.79; 95% CI: 1.06 to 12.52; $p = 0.02$) and greater white matter hyperintensity volume ($z = -2.64$, $p = 0.01$). Both differences remained significant after multiple comparison correction (Table 3).

### Functional connectivity differences

Among 217 participants included in the rs-fMRI analyses, group ICA identified 20 large-scale functional brain networks (Supplementary Fig. 3a–d; spatial correlation overlap map Supplementary Fig. 4). Compared to those with absent CAC ($n = 121$), individuals with high CAC ($n = 96$) showed increased functional connectivity in the right hippocampus and parahippocampal gyrus ($k = 388$ voxels, peak coordinates +24, −14, −26, $F = 2.21$, $p$-FDRcorr = 0.0037, age-adjusted; Fig. 1A). When additionally

**Table 2 | Group differences in cognitive outcomes**

| Outcome measure | Total $n = 278$ | CAC = 0 $n = 151$ | CAC ≥ 300 $n = 127$ | *p*-value | *p*-value FDR corr |
|---|---|---|---|---|---|
| Memory domain | 0.02 (0.94) | 0.21 (0.91) | −0.19 (0.93) | 0.30 | 0.30 |
| Missing | 1 | 1 | 0 | | |
| Executive domain | 0.03 (0.77) | 0.21 (0.73) | −0.18 (0.77) | 0.03* | 0.06 |
| Missing | 6 | 2 | 4 | | |
| Information processing | 0.04 (0.77) | 0.17 (0.76) | −0.12 (0.76) | 0.16 | 0.20 |
| Missing | 4 | 1 | 3 | | |
| Manual dexterity[a] | 0.22 (1.19) | 0.38 (0.96) | −0.06 (1.05) | 0.04* | 0.06 |
| Missing | 2 | 0 | 2 | | |
| G-Factor | 0.02 (1.00) | 0.29 (0.91) | −0.32 (1.00) | 0.01* | 0.04* |
| Missing | 8 | 2 | 6 | | |

*CAC* coronary artery calcium, *FDR corr* false discovery rate correction, *G-factor* general cognition composite.
[a]Median (interquartile range) of *z*-scored variable, significance test run on log-transformed and *z*-scored variables; mean (standard deviation) otherwise.
*$p$-value < 0.05.

adjusting for sex, a significant cluster emerged in the left precentral and postcentral gyri ($k = 244$ voxels, peak −48, −14, +34, $F = 1.88$, $p$-FDRcorr = 0.0038; Fig. 1B); adding sex as a covariate uncovered a hidden effect in the sensorimotor cortex that was previously masked by the strong imbalance of males in the high CAC group. These differences remained after further controlling for white matter hyperintensities, although the cluster size was reduced ($k = 116$ voxels, same peak, $F = 1.88$, $p$-FDRcorr = 0.013; Fig. 1C).

Seed-to-voxel analyses revealed greater connectivity in the high CAC group between the hippocampal/parahippocampal cortex and both the bilateral temporal poles ($h^2 = 1.14$, age-adjusted) and the right insular cortex ($h^2 = 0.57$, age-adjusted). The right putamen also showed stronger connectivity with the salience network ($h^2 = 0.35$, age-adjusted) and the visual network ($h^2 = 0.38$, age-adjusted). In contrast, individuals with absent CAC exhibited greater connectivity between the right putamen and the dorsal attention network ($h^2 = -0.31$, age-adjusted). Connectivity effect sizes are reported in Supplementary Fig. 5-7. After adjusting for age, sex, and white matter hyperintensities, participants with high CAC showed greater connectivity between the left precentral/postcentral cortex and the frontoparietal ($h^2 = 0.09$), language ($h^2 = 0.17$), visual ($h^2 = 0.04$), and sensorimotor networks ($h^2 = 1.45$).

Post hoc ROI-to-ROI analyses revealed significant group differences in functional connectivity involving the right putamen and right hippocampus/parahippocampal region. As shown in Fig. 2, participants with high CAC exhibited hypoconnectivity between the right putamen and several left-hemisphere networks, including the salience (RPFC, $T = -2.51$, $p$-FDRcorr = 0.013), frontoparietal (PPC, $T = -2.54$, $p$-FDR = 0.012), language (pSTG, $T = -2.06$, $p$-FDRcorr = 0.041), and dorsal attention networks (IPS, $T = -2.24$, $p$-FDRcorr = 0.026), as well as a second salience region (SMG, $T = -1.99$, $p$-FDRcorr = 0.048). In contrast, hyperconnectivity was observed between the right putamen and the right hippocampus ($T = 2.59$, $p$-FDRcorr = 0.01). Figure 3 depicts additional hypoconnectivity between the right hippocampus/parahippocampal cortex and left-hemisphere regions, including the language network (pSTG, $T = -2.23$, $p$-FDR = 0.027), the dorsal attention network (IPS, $T = -2.10$, $p$-FDRcorr = 0.037), and both anterior and posterior divisions of the parahippocampal gyrus with the left frontoparietal network (LPFC: $T = -2.29$, $p$-FDRcorr = 0.023; PPC: $T = -2.04$, $p$-FDRcorr = 0.043). These findings underscore distinct network-level alterations in individuals with high CAC, particularly affecting cortico-limbic and attentional circuits.

### Cerebral blood flow

Among 194 participants with arterial spin labeling data, only the inferior frontal gyrus pars opercularis showed significantly reduced perfusion in the high CAC group compared to the absent group (adjusted mean difference = −3.33; 95% CI: −6.54 to −0.12; $p = 0.042$), in models adjusting for age and sex. Models not adjusted for age and sex indicated lower perfusion in the precuneus (adjusted mean difference = −3.90; 95% CI: −7.32 to −0.48; $p = 0.049$), cuneal cortex (adjusted mean difference = −5.59; 95% CI: −9.75 to −1.44; $p = 0.010$), temporal fusiform and temporal-occipital fusiform cortex (adjusted mean difference = −3.16; 95% CI: −6.33 to 0.02; $p = 0.035$ and adjusted mean difference = −3.80; 95% CI: −7.06 to −0.54; $p = 0.006$ respectively), occipital gyri (adjusted mean difference = −3.93; 95% CI: −7.67 to −0.19; $p = 0.033$), and bilateral thalami (R: adjusted mean difference = −3.97; 95% CI: −7.05 to −0.90; $p = 0.019$; L: adjusted mean difference = −3.64; 95% CI: −6.68 to −0.60; $p = 0.016$). Results are presented in Table 4, and group-averaged perfusion maps are shown in Fig. 4. Effect sizes of all significant results are reported in Supplementary Table 5.

### Smoking as covariate

We conducted sensitivity analyses adjusting for current smoking status in all primary models. Results were unchanged: the g-factor difference remained significant ($p = 0.004$), as did total brain volume ($p = 0.030$), white matter hyperintensity volume ($p = 0.010$), and hippocampal connectivity ($p$-FDR = 0.004). The left sensorimotor cortex connectivity cluster remained significant but with further reduced spatial extent ($k = 98$ voxels; $p$-FDR = 0.02). Given that smoking is likely part of the causal pathway linking CAC to brain outcomes (rather than a pure confounder), we decided not to include it as a mandatory covariate in primary models to avoid overadjustment bias. Results are reported in Supplementary Table 6.

## Discussion

The main findings were: (1) cognitively unimpaired adults with high coronary artery calcification (CAC) showed lower general cognitive performance, although no group differences emerged in domain-specific cognitive performance indicating that the relation with cognitive performance is not strong; (2) significant alternations were observed in brain structure and functional organization, and only in one region for cerebral blood flow; (3) no group differences were found in serum biomarkers related to Alzheimer's disease, neurodegeneration and astrocyte activation, systemic inflammation, or lipids profiles. These results suggest that coronary calcification may contribute to early cognitive and cerebrovascular changes independent of Alzheimer's disease when measured through Alzheimer's disease-related blood biomarkers.

Previous studies have reported differences in specific cognitive domains among cognitively unimpaired individuals with varying CAC scores[12–14,35], although our results did not reveal such differences after correcting for multiple comparisons. These discrepancies likely reflect

**Table 3 | Group differences in serum and brain volumetric outcomes**

| Outcome measure | Total *n* = 278 | CAC = 0 *n* = 151 | CAC ≥ 300 *n* = 127 | *p*-value | *p*-value FDR corr |
|---|---|---|---|---|---|
| Aβ42/Aβ40[a] | 0.06 (0.02) | 0.06 (0.01) | 0.06 (0.01) | 0.08 | 0.24 |
| Missing | 5 | 2 | 3 | | |
| pTau181[a] | 24.26 (13.9) | 23.1 (14.1) | 25.6 (12.7) | 0.59 | 0.89 |
| Missing | 8 | 4 | 4 | | |
| GFAP[a] | 100.99 (68.3) | 103.7 (65.8) | 99.4 (72.0) | 0.01* | 0.06 |
| Missing | 4 | 2 | 2 | | |
| NfL[a] | 18.51 (11.1) | 17.7 (10.5) | 19.7 (11.3) | 0.92 | 0.92 |
| Missing | 4 | 2 | 2 | | |
| Cholesterol[b] | 5.4 (1.40) | 5.50 (1.49) | 5.34 (1.21) | 0.91 | 0.91 |
| Missing | 8 | 3 | 5 | | |
| HDL[b] | 1.40 (0.50) | 1.48 (0.60) | 1.40 (0.43) | 0.02* | 0.06 |
| Missing | 8 | 3 | 5 | | |
| LDL | 3.29 (0.93) | 3.33 (0.94) | 3.24 (0.91) | 0.45 | 0.68 |
| Missing | 8 | 3 | 5 | | |
| Triglyceride[b] | 1.55 (0.81) | 1.51 (0.87) | 1.57 (0.75) | 0.87 | 0.91 |
| Missing | 9 | 4 | 5 | | |
| Non fasting glucose[b] | 5.70 (0.90) | 5.60 (0.93) | 5.80 (1.00) | 0.01* | 0.06 |
| Missing | 9 | 7 | 2 | | |
| IL6[b] | 1.64 (1.35) | 1.55 (1.10) | 2.04 (1.46) | 0.02* | 0.06 |
| Missing | 17 | 9 | 8 | | |
| CRP[b] | 1.10 (1.47) | 1.20 (1.50) | 1.10 (1.40) | 0.77 | 0.91 |
| Missing | 11 | 6 | 5 | | |
| TNFa[b] | 0.60 (2.88) | 0.58 (0.34) | 0.65 (0.41) | 0.15 | 0.27 |
| Missing | 1 | 1 | 0 | | |
| IL1B[b] | 0.05 (0.03) | 0.04 (0.03) | 0.05 (0.06) | 0.09 | 0.20 |
| Missing | 3 | 3 | 0 | | |
| | **n = 222** | **n = 124** | **n = 98** | ***p*-value** | ***p*-value FDR corr** |
| Total brain (ml) | 1119.15 (20.94) | 1120.81 (21.36) | 1117.03 (20.32) | 0.02* | 0.02* |
| Total WMH[a](ml) | 2.11 (3.40) | 1.61 (2.73) | 2.58 (4.58) | 0.01* | 0.02* |

[a]Median (interquartile range) and ANCOVA run on log-transformed and z-scored variables; mean (standard deviation) otherwise.
[b]Median (interquartile range) and Mann–Whitney.
*$p$-value < 0.05.
*Aβ* amyloid-beta, *CAC* coronary artery calcium, *CRP* C-Reactive Protein, *FDR corr* false discovery rate correction, *GFAP* glial fibrillary acid protein, *HDL* high-density lipoprotein, *IL-1β* interleukin-1 beta, *IL-6* interleukin-6, *LDL* low-density lipoprotein, *NfL* neurofilament light, *pTau* phosphorylated Tau, *TNF-α* tumor necrosis factor-alpha, *WMH* white matter hyperintensity.

methodological differences, including CAC group definitions and sample characteristics such as age. For example, Suemoto et al. found only weak associations between CAC and executive function, with no observed relationships for global cognition, delayed memory, or verbal fluency[13]. Their sample included participants with a mean age of 50 in the low CAC group and 60 in the high CAC group, whereas ours was 67 and 70 years, respectively. Moreover, they defined low CAC as <100, while we compared individuals with absent calcification (score = 0) to those with high calcification (score ≥ 300). We specifically chose this grouping since scores above 300 have been associated with significantly increased cardiovascular risk[11]. Using this threshold aligns our findings more closely with clinical workflows. Similarly, Reis et al. studied a sample aged 43–55 years, illustrating how demographic differences might influence results[14].

The observation of lower general cognitive performance (g-factor) in the high CAC group, in the absence of domain-specific deficits and with preserved MMSE scores, warrants careful interpretation. This pattern is consistent with early, subtle cognitive inefficiency rather than frank impairment. The g-factor, by aggregating data across multiple tests, may capture variance related to processing robustness, attentional consistency, or cognitive reserve that individual domain scores, each with lower reliability and higher task-specific variance, fail to detect. In contrast, MMSE is a brief screening tool designed to detect dementia-range impairment and is insensitive to the mild differences observed here. Importantly, our findings do not indicate clinical cognitive impairment; rather, they suggest statistically lower cognitive performance in individuals with high CAC. Whether this difference represents an early marker of accelerated cognitive aging, a stable individual difference, or residual confounding requires longitudinal replication. The absence of domain-specific deficits does not contradict the g-factor finding, as such effects may not yet be detectable in cognitively unimpaired individuals. Increasing evidence suggests that traditional cognitive assessment tools may lack sensitivity to detect these early changes, highlighting the potential value of more sensitive approaches such as digital cognitive assessment (see Polk et al. for a review)[36].

Our findings suggest that high CAC is associated with measurable brain changes in the absence of elevated Alzheimer's disease biomarkers, supporting a vascular pathway to early cognitive vulnerability. Specifically, we found increased white matter hyperintensities and reduced brain volume in individuals with high CAC compared to those with absent CAC, consistent with structural changes linked to vascular burden[17,37]. Functional neuroimaging further revealed altered connectivity, including increased connectivity between the right hippocampal/parahippocampal cortex and sensorimotor regions, reduced connectivity between subcortical regions and key cognitive networks (frontoparietal, salience, language, and dorsal attention networks), and increased connectivity between limbic and subcortical regions.

The resting state functional neuroimaging results varied depending on the covariates used in the models. The emergence of the left sensorimotor cortex cluster only after adjusting for sex (Fig. 1B, C) illustrates a classical suppression effect. Males were substantially overrepresented in the high CAC group (75% vs. 46% in the absent CAC group). Because male sex is independently associated with both higher CAC and, in this sample, lower sensorimotor connectivity, the unadjusted model contained opposing effects: the positive association between CAC and connectivity was partially masked by the negative association between male sex and connectivity. Adding sex as a covariate removed this "noise" and revealed the CAC-connectivity relationship. This statistical pattern, rather than indicating confounding, suggests that the true effect of CAC on sensorimotor connectivity is even stronger than apparent in raw comparisons. Notably, the sensorimotor hyperconnectivity observed here aligns with prior work demonstrating altered sensorimotor network organization in individuals with elevated vascular risk[38]. More broadly, regional hyperconnectivity, affecting both sensorimotor and limbic circuits, has been observed across multiple studies of individuals with vascular burden who remain cognitively intact, with hippocampal hyperconnectivity specifically linked to white matter hyperintensity burden in preclinical populations[37]. That this relationship emerged only after accounting for sex underscores the importance of considering demographic factors when investigating the compensatory or maladaptive plasticity that may accompany early-stage vascular burden. In this context, increased connectivity, particularly within sensorimotor circuits, has been proposed as a potential mechanism to maintain behavioral performance despite subtle vascular compromise, reflecting network-level cognitive reserve[39]. The co-occurrence of reduced CBF in frontal regions alongside sensorimotor hyperconnectivity in the same individuals further supports the interpretation that these phenomena represent parallel processes, wherein some networks upregulate synchrony to compensate for

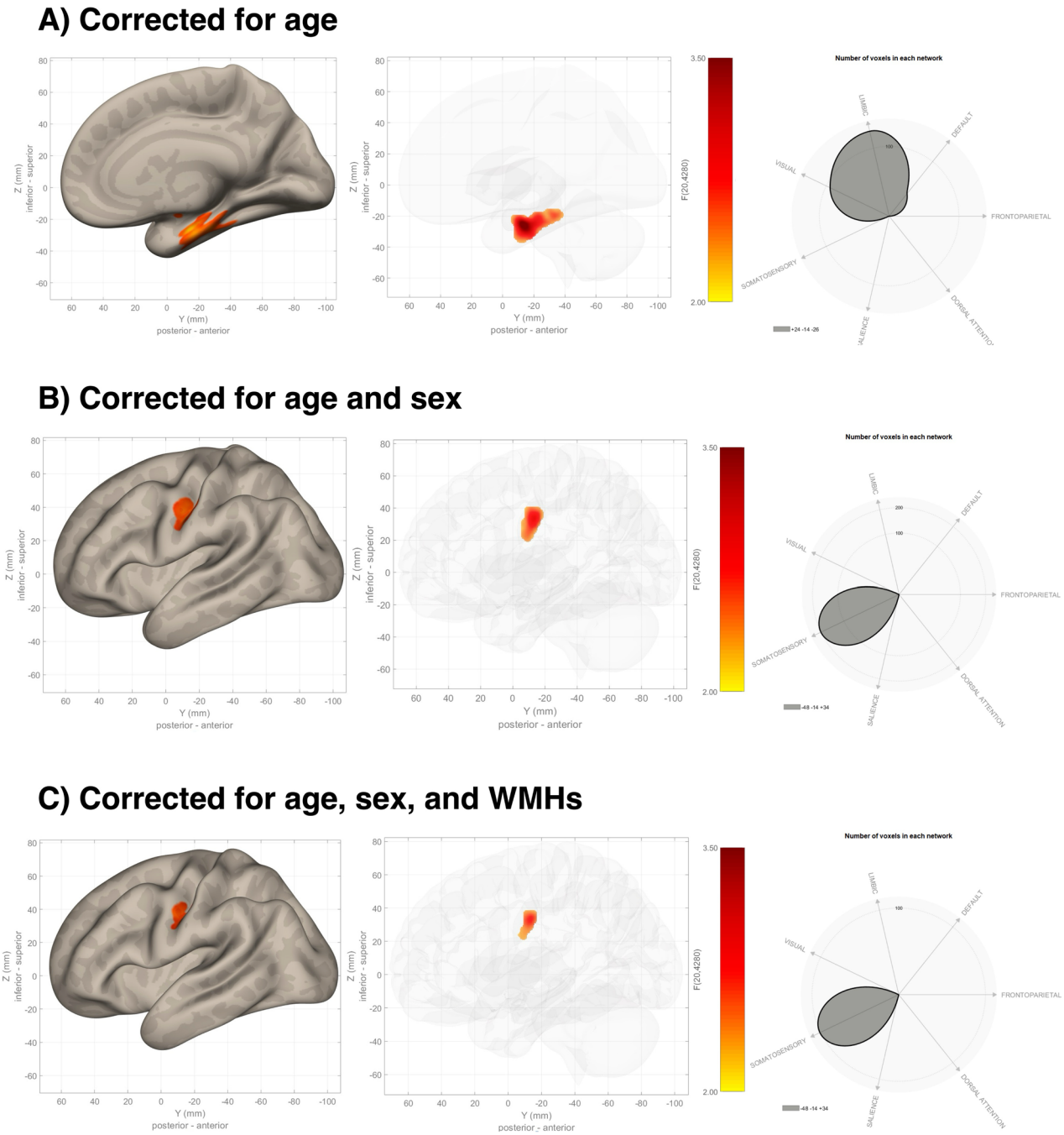


**Fig. 1 | Regions with greater connectivity in high versus absent CAC.** Second-level seed-to-voxel analyses comparing participants with high versus absent coronary artery calcification (CAC), controlling for age (**A**), age and sex (**B**), and age, sex, and white matter hyperintensity volume (**C**). Each panel displays clusters showing significantly increased connectivity strength in the high CAC group, overlaid on a surface-rendered brain and corresponding glass-brain projection. Statistical thresholds were set at voxel-level $p < 0.001$ (uncorrected) and cluster-level $p$-FDR < 0.05. **A** shows a significant cluster centered in the right hippocampal/parahippocampal cortex. **B**, **C** reveal overlapping clusters in the left precentral and postcentral gyri, with reduced spatial extent in panel C following adjustment for white matter hyperintensity (WMH). Accompanying radar plots show the functional connectivity profile of each cluster across canonical networks defined in the CONN toolbox (e.g., sensorimotor, salience, visual, frontoparietal).

vascular insult while others show overt hypoperfusion. Whether this sensorimotor hyperconnectivity ultimately proves protective (slowing cognitive decline) or pathological (predicting future network failure) will require longitudinal investigation.

These network alterations may suggest a shift in brain functional organization that may precede hemodynamic changes, as our arterial spin labeling findings showed only trends toward reduced CBF in individuals with high CAC, with the most robust effect in the inferior frontal gyrus pars opercularis (after adjusting for age and sex). Although temporal claims should be taken cautiously, since this was a cross-sectional study. After covariate adjustment and multiple comparison correction, only a single region, the inferior frontal gyrus pars opercularis, showed significantly reduced perfusion in the high CAC group, despite widespread differences before multiple comparison correction. Several non-mutually exclusive explanations may account for this pattern. First, cerebral autoregulation maintains stable CBF across a wide range of perfusion pressures; this homeostatic mechanism may effectively buffer against moderate, chronic reductions in cardiac output associated with subclinical coronary

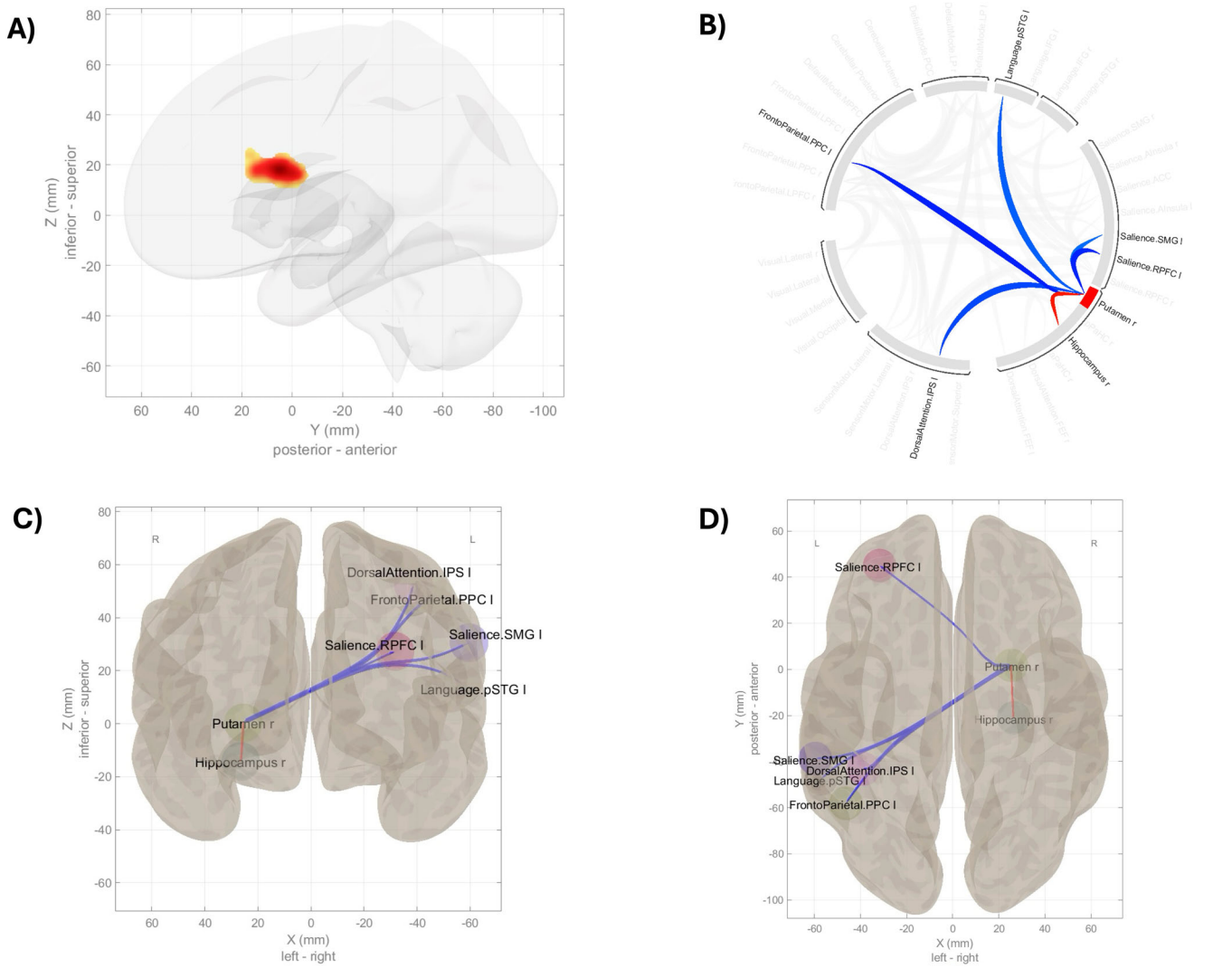


**Fig. 2 | ROI-to-ROI connectivity differences from the right putamen (high CAC > absent CAC).** Post hoc ROI-to-ROI analysis using the right putamen—identified via seed-to-voxel analysis—as the seed region. **A** Cluster location visualized on a glass-brain rendering. **B** Circular connectogram showing significant between-group connectivity differences. Blue edges represent hypoconnectivity (reduced connectivity in the high CAC group); red edges indicate hyperconnectivity (increased connectivity). **C**, **D** 3D cortical surface renderings of the spatial distribution of significant ROI-to-ROI connections. High CAC was associated with reduced connectivity between the right putamen and left-hemisphere ROIs in the salience (RPFC, SMG), frontoparietal (PPC), dorsal attention (IPS), and language (pSTG) networks, and increased connectivity with the right hippocampus. All results reflect second-level GLM contrasts, FDR-corrected at the connection level ($p$-FDR < 0.05).

atherosclerosis. The focal vulnerability of the inferior frontal gyrus pars opercularis could reflect regionally specific hemodynamic properties, such as its location at distal arterial border zones (watershed areas) that are particularly sensitive to hypoperfusion. Second, the cross-sectional design captures a single time point; individuals with high CAC may have exhibited more widespread CBF reductions earlier in the disease process, but compensatory vascular remodeling (e.g., collateralization) could have partially restored perfusion by the time of assessment. Third, statistical power for detecting regional CBF differences is constrained by the combination of moderate sample size and ASL signal-to-noise limitations. Longitudinal ASL studies are needed to elucidate CBF trajectories in this sample.

To determine whether findings reflected Alzheimer's disease-related mechanisms, we examined serum biomarkers of amyloid, tau, and neurodegeneration, as well as peripheral inflammatory and lipid markers. No group differences were observed, supporting a vascular rather than Alzheimer's-specific pathway; however, systemic markers may fail to capture localized cerebrovascular changes and other markers may need to be used as outlined below.

Our findings offer translational recommendations with potential implications for risk stratification, clinical monitoring, and design of future intervention trials. Results collectively show subtle cognitive differences, structural brain changes (increased white matter hyperintensities, reduced brain volume), functional network alterations, and focal hypoperfusion, painting a picture of early vascular brain changes. This pattern suggests that subclinical coronary atherosclerosis is not a silent bystander but an active contributor to brain vulnerability, offering a critical window for intervention before the onset of significant cognitive decline.

Our results indicate that a CAC score of 300 or greater, a threshold already used clinically to denote severe coronary atherosclerosis and high cardiovascular disease risk, may also serve as a practical "red flag" for early brain changes in cognitively normal adults. This is an important finding since CAC scoring is a non-invasive, widely available, and standardized test. Leveraging this existing clinical metric could provide a cost-effective strategy to identify a subset of the population at heightened risk for vascular brain injury, even in the absence of overt cognitive symptoms. We therefore

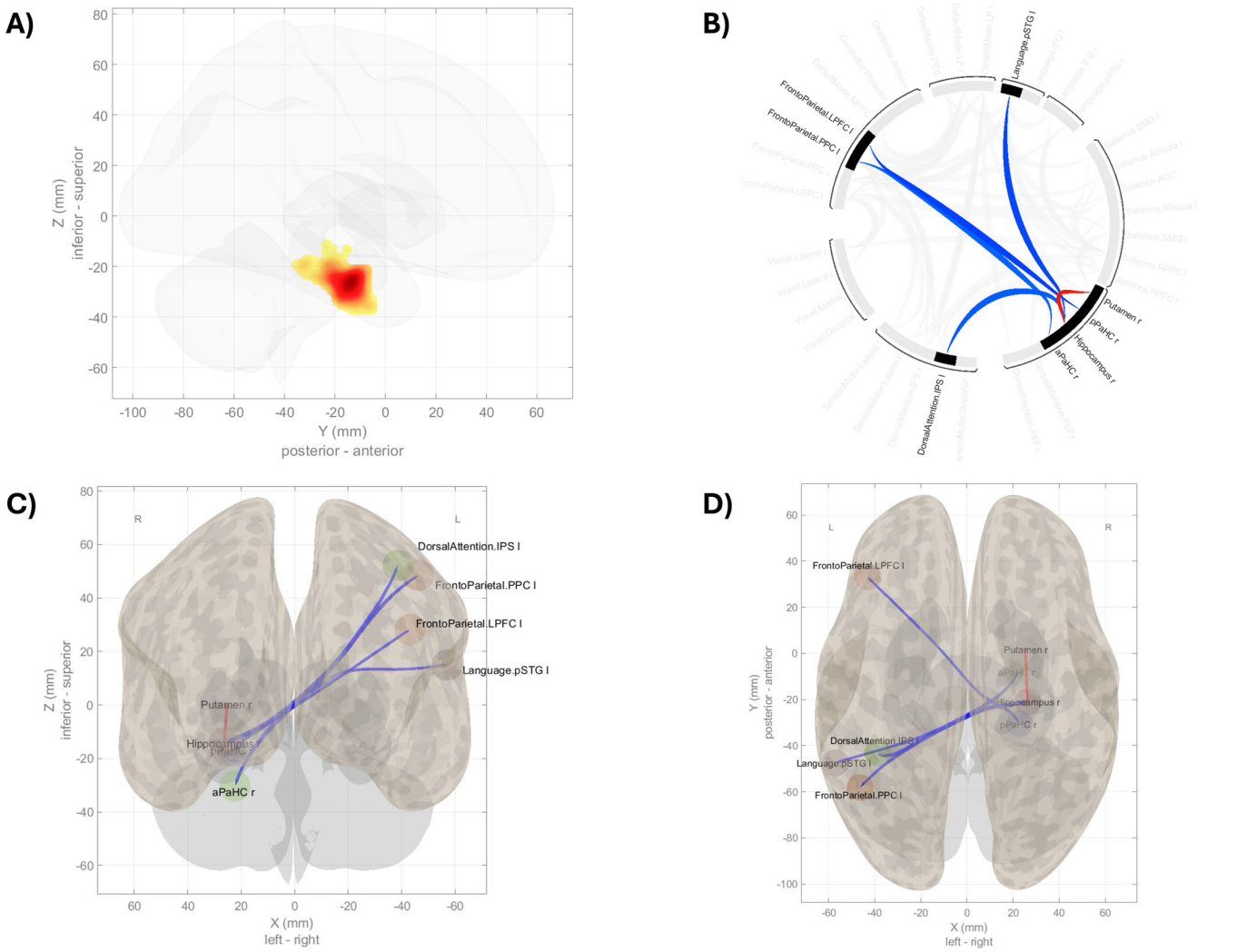


**Fig. 3 | ROI-to-ROI connectivity differences from the right hippocampal/parahippocampal cortex (high CAC > absent CAC).** Post hoc ROI-to-ROI analysis using the right hippocampal/parahippocampal cortex, identified via seed-to-voxel analysis, as the seed region. **A** Cluster location visualized on a glass-brain rendering. **B** Circular connectogram showing significant between-group connectivity differences. Blue edges represent hypoconnectivity (reduced connectivity in the high CAC group); red edges indicate hyperconnectivity (increased connectivity). **C**, **D** 3D cortical surface renderings of the spatial distribution of significant ROI-to-ROI connections. High CAC was associated with reduced connectivity between the right hippocampal/parahippocampal cortex and left-hemisphere ROIs in the frontoparietal (LPFC, PPC), language (pSTG), and dorsal attention (IPS) networks, and increased connectivity with the right putamen. All results reflect second-level GLM contrasts, FDR-corrected at the connection level ($p$-FDR < 0.05).

propose that a CAC score of 300 or greater should prompt clinicians to broaden their risk assessment from a focus solely on myocardial infarction and stroke to include the brain as a key target organ for vascular damage.

This subgroup may be an ideal population for targeted cognitive baseline assessment, using either sensitive, validated neuropsychological instruments or emerging digital assessments that offer greater ecological validity and sensitivity to subtle variation, as well as serial monitoring of vascular risk factors. A high CAC score signals a need for optimized management of all modifiable risk factors (e.g., hypertension, dyslipidemia, diabetes, smoking), a focus that could serve as a powerful motivator for both patients and clinicians to adhere to preventive strategies. Finally, while not yet a clinical recommendation, this population may be a suitable candidate for research studies utilizing advanced cerebrovascular imaging (e.g., intracranial vessel wall imaging, cerebrovascular reactivity testing) to directly assess whether peripheral coronary calcification parallels cerebral vessel involvement.

Our findings also have implications for clinical trial design, suggesting that cognitively normal individuals with a CAC score of 300 or greater should be prioritized for recruitment into vascular risk reduction trials aimed at preserving cognitive function. This group represents a high-value target since they exhibit measurable brain changes consistent with a vascular etiology, enriching the sample for the target pathology and increasing the likelihood of detecting a treatment effect. At the same time, this group would offer a defined mechanistic pathway where the primary driver of brain change is likely vascular, allowing for the testing of targeted interventions (such as intensive lipid-lowering, anti-hypertensive regimens, or novel agents that improve endothelial function) with a clear mechanistic rationale. Furthermore, the feasibility of enrollment is high because CAC scoring is a common clinical tool, making this population practical to identify and recruit. Trials in this group could leverage a combination of outcomes, including primary endpoints like change in a sensitive measure of general cognitive ability or performance on digital cognitive assessments, as well as surrogate endpoints such as progression of white matter hyperintensities on MRI, changes in cerebral blood flow measured with ASL, or normalization of functional network connectivity. These imaging biomarkers could provide evidence for a drug's efficacy in a shorter, smaller trial before moving to large-scale cognitive

**Table 4 | Cerebral blood flow differences**

| Region of interest | Total $n = 194$ | CAC = 0 $n = 113$ | CAC ≥ 300 $n = 81$ | *p*-value | *p*-value[a] |
|---|---|---|---|---|---|
| Total brain | 37 (8) | 38 (7) | 36 (8) | 0.050 | 0.549 |
| Inferior frontal gyrus pars opercularis | 51 (11) | 53 (10) | 49 (12) | 0.004* | 0.042* |
| Middle temporal gyrus temporooccipital part | 48 (13) | 50 (12) | 46 (14) | 0.068 | 0.319 |
| Postcentral gyrus | 43 (10) | 44 (9) | 42 (12) | 0.200 | 0.941 |
| Superior parietal lobule | 35 (12) | 36 (11) | 33 (13) | 0.082 | 0.763 |
| Missing | 4 | 2 | 2 | | |
| Angular gyrus | 51 (11) | 52 (11) | 50 (12) | 0.400 | 0.888 |
| Cingulate gyrus posterior division | 53 (13) | 55 (11) | 52 (15) | 0.100 | 0.688 |
| Precuneus cortex | 45 (12) | 47 (12) | 43 (12) | 0.049* | 0.469 |
| Cuneal cortex | 44 (15) | 46 (14) | 40 (15) | 0.010 | 0.148 |
| Temporal fusiform cortex posterior division | 32 (11) | 33 (12) | 30 (10) | 0.035* | 0.361 |
| Temporal occipital fusiform cortex | 41 (11) | 43 (10) | 39 (13) | 0.006* | 0.165 |
| Occipital fusiform gyrus | 44 (13) | 45 (12) | 41 (14) | 0.033* | 0.288 |
| Left thalamus | 37 (11) | 38 (10) | 35 (11) | 0.016* | 0.327 |
| Left hippocampus | 39 (9) | 40 (8) | 39 (10) | 0.400 | 0.727 |
| Left amygdala | 37 (8) | 38 (8) | 36 (8) | 0.110 | 0.248 |
| Right thalamus | 37 (11) | 38 (11) | 34 (10) | 0.019* | 0.370 |
| Missing | 1 | 1 | 0 | | |
| Right hippocampus | 39 (10) | 40 (9) | 38 (10) | 0.200 | 0.961 |
| Right amygdala | 35 (8) | 35 (9) | 34 (8) | 0.400 | 0.584 |

[a]Analyses corrected for age and sex. Means (standard deviations) are reported.
*$p$-value <0.05. CBF in mL/100 g/min.

endpoint studies. Also, adding cerebral perfusion outcomes in trials has been shown to increase the understanding of intervention's effects[40], which may be particularly relevant in this sample.

Several future directions can be identified for each methodology. First, longitudinal imaging studies are needed to determine whether the connectivity alterations we observed predict cognitive decline over time. Second, vascular-specific biomarkers, such as placental growth factor (PlGF) and vascular endothelial growth factor (VEGF), may outperform generic inflammatory markers in capturing the mechanistic pathways linking CAC to early neurovascular changes, as they have shown predictive value for Alzheimer's disease progression in cognitively unimpaired individuals (i.e., over 12 years of follow-up)[41]. Third, digital cognitive assessments with greater ecological validity could enhance the detection of subtle domain-specific variation in this population. Fourth, high-resolution cerebrovascular imaging to directly examine intracranial atherosclerotic burden would clarify whether peripheral calcification parallels cerebral vessel involvement.

This study has limitations. Women were underrepresented in the high CAC group, and we did not assess carotid or intracranial atherosclerosis, which may also contribute to brain changes. The imaging and CAC assessments were separated by an average of 2.6 years, though CAC is a stable marker over time, and analyses were corrected for the time interval between assessments. While plasma is the most commonly used matrix in the literature for these biomarkers, this study used serum due to sample availability. Nevertheless, previous work has demonstrated that serum measurements for these markers are reliable and clinically meaningful[28]. We verified that all serum biomarker concentrations were well above the limits of quantification for the respective assays, ensuring measurement validity. A limitation of arterial spin labeling includes its inherent susceptibility to noise, motion, and partial volume effects, particularly in small or deep gray matter regions, which may reduce the sensitivity for detecting subtle perfusion changes. Furthermore, cerebral autoregulatory mechanisms may buffer against early perfusion alterations associated with CAC reduction, potentially masking early cerebrovascular impacts. Also, we did not include emerging biomarkers such as p-tau217 or those specific to vascular dementia[42]. Nonetheless, the great strength of the study is the assessment of several, multi-modal markers in a population with defined coronary artery calcification scores.

Taken together, our findings suggest that high coronary artery calcification may signal early cerebrovascular dysfunction and reduced cognitive reserve in cognitively unimpaired adults. The integration of advanced neuroimaging and cardiovascular screening may enhance early detection of individuals at risk for cognitive decline through non-Alzheimer's pathways.

## Methods

### Participants

A total of 285 cognitively unimpaired adults aged 50 years or older were recruited from the Lifelines cohort, a large population-based study conducted in the Netherlands. All participants had previously undergone non-contrast cardiac computed tomography (CT) as part of the Imalife substudy[43] between September 2017 and March 2022. Individuals were invited to the current Memolife study if they met the following inclusion criteria: (i) no history of vascular, neurological, or psychiatric disorders within the prior two years, (ii) no contraindications for MRI, and (iii) a Mini-Mental State Examination (MMSE) score ≥ 25. Ethical approval was granted by the Medical Ethics Review Board of the University Medical Center Groningen (approval NL70343.042.20, 26-11-2020), and all participants provided written informed consent. An overview of the Memolife study procedures and variables is displayed in Supplementary Fig. 1, and participants' inclusion flow in Supplementary Fig. 2.

### Study design and procedures

Eligible participants completed neuropsychological testing and blood sampling during a single on-site visit at the University Medical Center Groningen between February 2021 and November 2022. MRI scanning was performed on a separate day (between March 2022 and November 2023). The mean interval between CT and MRI assessments was 2.6 ± 1.1 years.

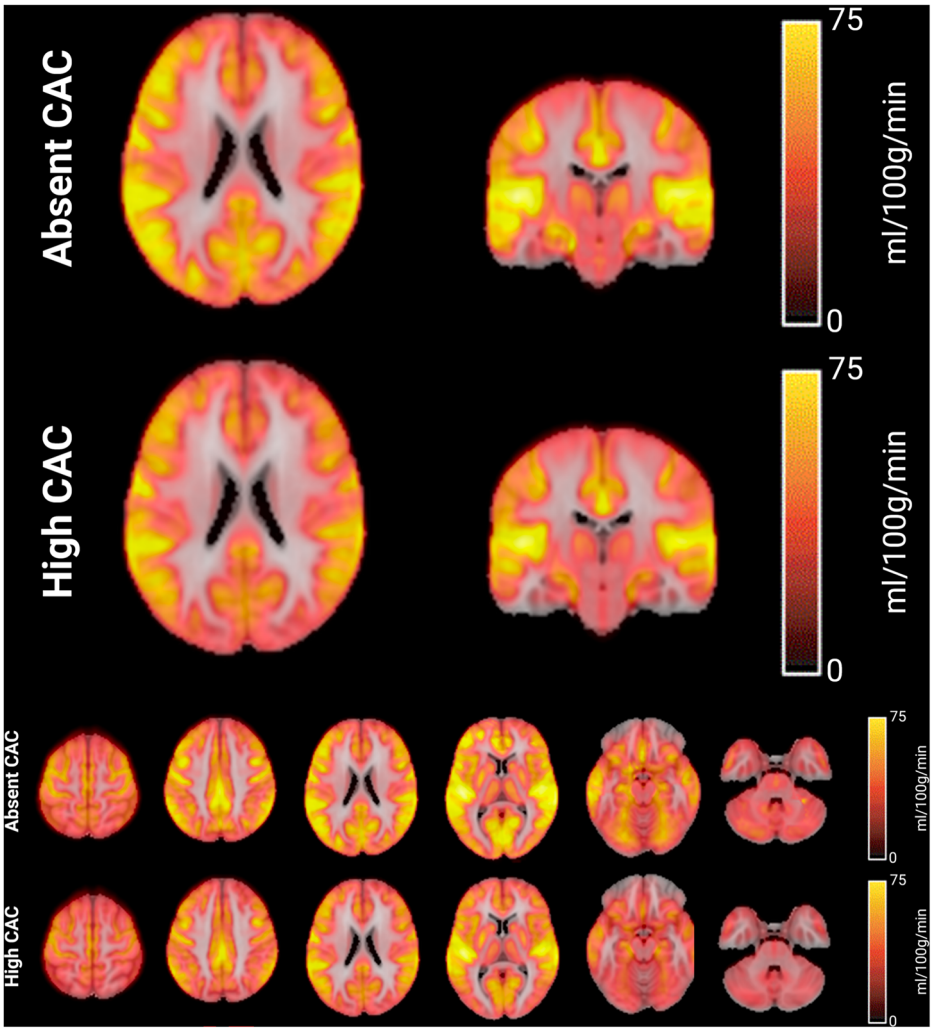


**Fig. 4 | Group-mean CBF maps in MNI152 2 mm space for participants with absent (top) and high (bottom) coronary artery calcification (CAC).** Representative cerebral blood flow (CBF) maps in standard space derived from vessel-encoded pseudocontinuous arterial spin labeling (VEPCASL). Scale bar on the right represents perfusion values in mL/100 g/min. Visual comparison suggests regionally lower CBF in the high CAC group, particularly in posterior cortical and subcortical regions. Each subject's calibrated CBF map was nonlinearly registered to MNI152 2 mm space and averaged within group for visualization. Quantitative analyses (see Table 4) revealed that, after adjusting for age and sex, only the *inferior frontal gyrus pars opercularis* showed significantly reduced perfusion in the high CAC group ($p = 0.042$). Several additional regions, including the precuneus, cuneal cortex, temporal and occipital fusiform gyri, and bilateral thalami, showed reduced perfusion only when not correcting for age and sex.

### Coronary artery calcification

Coronary artery calcium (CAC) was assessed using non-enhanced third-generation dual-source CT (Somatom Force, Siemens Healthineers). The Agatston score was computed to quantify CAC burden[44]. Further information on these procedures has been published elsewhere[35,43]. Participants were stratified into two groups following previously reported recommendations[11]: those with no detectable CAC (score = 0) and those with high CAC (score ≥ 300).

### Cognitive assessment

Neuropsychological testing was conducted using standardized protocols and included the following assessments: Mini Mental State Examination (MMSE)[45], Auditory Verbal Learning Test (AVLT, immediate and delayed recall)[46,47], Trail Making Test A and B (TMT A and TMT B)[48], Purdue Pegboard Test[49], Letter Digit Substitution Test (LDST)[50], Visual Association Test (VAT)[51], Digit Span Forward and Backward[52], Stroop Color-Word Test[53], and Animal Verbal Fluency[54]. *Z*-scores were calculated for each test. From these, domain composite scores for memory, executive function, information processing, and motor function were created by averaging z-scored individual test scores within each domain, following a method previously used[55]. Lower scores reflect poorer performance. The memory domain comprised AVLT immediate and delayed recall. Executive function included the Stroop Color–Word Test interference score, Animal Verbal Fluency, and the LDST (weighted half). Information processing speed included the LDST (weighted half) and the Stroop Color–Word Test Parts I and II. For time-based measures where higher values indicated poorer performance (Stroop interference and Stroop Parts I and II), scores were multiplied by −1 so that higher *z*-scores consistently reflected better performance across all measures. Manual dexterity was assessed using the Purdue Pegboard Test (sum of right-hand and left-hand trials).

Additionally, a general cognitive composite (g-factor) was derived using principal component analysis, extracting the first unrotated component, which explained 50.3% of the total variance and showed positive loadings (>0.40) across tests. The g-factor provides a summary measure of shared variance across cognitive domains, thereby increasing sensitivity to subtle differences in overall cognitive function. The MMSE was not included in the derivation of the g-factor due to restricted range and ceiling effects in this cohort (all participants ≥ 25; 80% scored 29–30) and is therefore reported separately for descriptive purposes. Detailed domain score calculations and g-factor derivation code are provided in the Supplementary Materials.

### Blood biomarker analysis

Blood was collected under non-fasting condition. A 4 mL serum sample was taken, centrifuged at 1800 × *g* for 5 min at room temperature (21 °C), and conserved in aliquots of 2 mL at −80 °C at the University Medical Centre Groningen laboratory. Inflammatory markers, namely Interleukin-1 beta (IL-1β), Interleukin-6 (IL-6), Tumor Necrosis Factor-alpha (TNF-α), C-Reactive Protein (CRP), and lipid markers, namely, High-Density Lipoprotein (HDL), Low-Density Lipoprotein (LDL), triglycerides, non-fasting blood glucose, were analyzed in the same laboratory.

Determination of the Alzheimer's biomarker was conducted at the Amsterdam University Medical Centers, Department of Laboratory

Medicine, Neurochemistry Laboratory. The following biomarkers were assessed: Amyloid beta 40 (Aβ40), Amyloid beta 42 (Aβ42), phosphorylated Tau 181 (pTau181), Neurofilament Light Chain (NfL), and Glial Fibrillary Acidic Protein (GFAP). For analyses, the Aβ42/Aβ40 ratio was used instead of the single values. All measurements were performed on a single molecule array (Simoa) HD-x analyzer platform, with the Neurology 4-plex E kit (Quanterix, USA) in monoplo and the P-tau181 V2.1 kit (Quanterix) in duplo, according to the manufacturer's instructions and predefined laboratory quality control procedures. Prior to measurement, samples were briefly thawed at room temperature and centrifuged for 10 min at 10,000 × *g*.

Alzheimer's disease biomarker samples were excluded if they did not meet prespecified assay validity criteria established by the laboratory. Specifically, excluded samples comprised: pTau181 concentrations below the functional lower limit of quantification (LLOQ) combined with a coefficient of variation (CV) > 20% ($n = 2$); pTau181 concentrations below the functional LLOQ without additional CV violation ($n = 1$); Aβ42 concentrations below the functional LLOQ ($n = 1$); samples flagged due to Simoa technical error ($n = 1$); samples with insufficient sample volume ($n = 2$; including one sample additionally flagged for technical error); and empty vials without caps ($n = 2$). These thresholds and exclusion criteria were determined a priori by the performing laboratory as part of assay validation. No additional post hoc outlier removal was performed.

As expected for serum biomarkers, distributions were right-skewed; therefore, log-transformation was applied prior to statistical analyses to improve distributional assumptions. In the results tables, the median and interquartile range were reported. ANCOVA models were run on the log-transformed and z-scored variables. Distributions pre and post-log-transformations are provided below and in Supplementary Fig. 8.

For contextual interpretation, we compared our sample's NfL and GFAP concentrations to established reference ranges from the Amsterdam Dementia Cohort (accessible at: https://mybiomarkers.shinyapps.io/Neurofilament/; https://mybiomarkers.shinyapps.io/GFAP/). As noted in Results, our participants' values fell predominantly within the 75th–90th percentile of cognitively unimpaired reference populations, consistent with the age range of our sample (mean 68 years).

### Structural MRI acquisition and processing

MRI scans were acquired on a 3.0 T MAGNETOM Prisma scanner (Siemens) with a 64-channel head coil. Sequences included T1-weighted MPRAGE, T2-FLAIR, resting-state functional MRI (rs-fMRI), and vessel-encoded pseudocontinuous arterial spin labeling (VEPCASL)[56]. Structural imaging parameters were the following: T1-weighted MPRAGE: TR 2300 ms, TE 2.26 ms, TI 900 ms, FA 8 degrees, FOV (read) 256 mm, voxel size 1.0 × 1.0 × 1.0 mm, Bandwidth 200 Hz/pixel, acquisition time 5 min 20 s. T2-FLAIR: TR 5000 ms, TE 392 ms, TI 1800 ms, FOV (read) 256 mm, voxel size 1.0 × 1.0 × 1.0 mm Bandwidth 592 Hz/Px, TA 5:12. Structural images were processed using the cNeuro platform (Combinostics, Tampere, Finland) for automated segmentation (133 brain regions segmented via a multi-atlas approach based on 79 manual atlases). Total brain volume and white matter hyperintensities were extracted and adjusted for intracranial volume, therefore, normalized (corrected) values were used. White matter hyperintensity segmentation was conducted on FLAIR images using a multi-stage method based on the Expectation–Maximization algorithm[32]. Results are reported according to the OHBM Committee on Best Practice in Data Analysis and Sharing (COBIDAS) on MRI guidelines. A schematic overview of the processing and analytical workflow of the MRI data is presented in Supplementary Fig. 9.

All T1-weighted and FLAIR segmentations were visually inspected by a trained rater (J.D.M.), blinded to CAC status. Scans with motion artifacts, incomplete brain coverage, or failed segmentation ($n = 7$) were excluded. For white matter hyperintensity segmentation, automatic outputs were overlaid on native FLAIR images and verified for anatomical plausibility; manual corrections were applied where necessary ($n = 12$) following established guidelines[57].

### Resting-state functional MRI

Resting-state fMRI data were preprocessed using CONN (v22.a)[58] and SPM12 (release 12.7771). The current preprocessing pipeline is described elsewhere[59] and summarized below. Functional and anatomical scans were coregistered, motion- and slice-time corrected, normalized to MNI space, segmented into grey matter, white matter, and CSF, and smoothed with an 8 mm FWHM Gaussian kernel. Outlier scans were identified using ART (framewise displacement >2 mm or global BOLD signal >9 SD). Denoising included regression of white matter and CSF signals (5 CompCor components each), motion parameters and their derivatives (12 total), outliers, session effects, and linear trends. BOLD signals were bandpass filtered (0.01–0.1 Hz), resulting in 273.6–524.2 effective degrees of freedom.

Group ICA identified 20 networks using subject-level singular value decomposition, group-level singular value decomposition, fast-ICA, and GICA3 back-projection. Group-level voxel-wise GLMs tested between-group connectivity differences, with significance based on cluster-level inference (voxel $p < 0.001$; $p$-FDR < 0.05). Post hoc ROI-to-ROI connectivity was assessed using Fisher-transformed correlations, with hierarchical clustering and FDR correction at connection and cluster levels. Seed-to-voxel and ROI-to-ROI analyses compared connectivity between CAC groups, controlling sequentially for age, sex, and white matter hyperintensity volume.

### Resting-state functional MRI and T1-weighted imaging preprocessing

Functional and anatomical data underwent several preprocessing steps: first, scans were coregistered to a reference image using a 6-parameter rigid body transformation and resampled to correct for motion and susceptibility interactions. Second, temporal misalignment between slices was corrected using sinc temporal interpolation. Third, outlier scans were identified with framewise displacement above 2 mm or global blood-oxygenated-level-dependent (BOLD) signal changes above 9 standard deviations using ART. Visual inspection of all T1 and FLAIR segmentations was performed, and manual correction of white matter hyperintensity maps was applied where needed. Fourth, data were normalized to MNI space, segmented into grey matter, white matter, and CSF, and resampled to 2 mm isotropic voxels using the SPM unified segmentation and normalization algorithm. Finally, spatial smoothing was applied using a Gaussian kernel of 8 mm full-width half-maximum (FWHM).

### Quality assessment and denoising

Quality assessment was done during the denoising step using automated quality assessment graphs provided by CONN and verified through carpet plots. Motion exclusion criteria were explicitly applied, with framewise displacement >2 mm leading to scan censoring. Functional data were denoised using a pipeline that included regression of potential confounding effects such as white matter timeseries (5 CompCor noise components), CSF timeseries (5 CompCor noise components), motion parameters and their first-order derivatives (12 factors), outlier scans (below 53 factors), session effects and their first-order derivatives (2 factors), and linear trends (2 factors) within each functional run. This was followed by bandpass frequency filtering of the BOLD timeseries between 0.01 Hz and 0.1 Hz. CompCor noise components were estimated by computing the average BOLD signal and the largest principal components orthogonal to the BOLD average, motion parameters, and outlier scans within each subject's eroded segmentation masks. The effective degrees of freedom of the BOLD signal after denoising ranged from 273.6 to 524.2, with an average of 522.2 across all subjects.

### First-level analysis

Group-level independent component analyses (group-ICA) identified 20 large-scale functional networks from the combined rs-fMRI data of all subjects. This process involved several steps: first, BOLD signals from every time point and voxel across subjects and conditions were concatenated along the temporal dimension. Next, a subject-specific singular value

decomposition with 64 components for each subject was used for initial dimensionality reduction, followed by a group-level singular value decomposition with 20 components for the concatenated data. Then, a fast-ICA fixed-point algorithm with a hyperbolic tangent (G1) contrast function was applied to identify spatially independent group-level networks from the reduced components. Finally, GICA3 back-projection was used to compute ICA maps for these networks separately for each subject.

All 20 components were retained and visually inspected for correspondence to canonical resting-state networks (Supplementary Fig. 3a–d). Components clearly corresponding to artifactual patterns (e.g., edge effects, white matter/CSF signal) were excluded from further analysis ($n = 3$), leaving 17 networks for statistical testing. The remaining 17 components were identified and labeled based on their spatial correlation with established resting-state network templates, with selection criteria involving maximization of Dice similarity coefficients with canonical network maps.

### Group-level analyses

Between-group comparisons were performed for each of the 17 networks using second-level voxel-wise General Linear Models (GLMs), with first-level connectivity measures as dependent variables and groups or subject-level identifiers as independent variables. Voxel-level hypotheses were evaluated using multivariate parametric statistics with random-effects across subjects and sample covariance estimation across multiple measurements.

To correct for multiple comparisons across all tested networks, we used a two-stage approach: (1) an initial voxel-level threshold of $p < 0.001$ (uncorrected), followed by (2) a cluster-level false discovery rate (FDR) correction at $p < 0.05$. This method controls for false positives while maintaining sensitivity in exploratory whole-brain analyses. Cluster-level inference was based on Gaussian Random Field theory. The rationale for seed selection in seed-to-voxel analyses is as follows: seeds were defined a priori as 6 mm spheres centered at the peak coordinates emerging from the ICA findings.

### Seed-to-voxel analyses

Seed-to-voxel analyses were conducted as hypothesis-driven follow-ups to the group ICA results. Seeds were defined as 6 mm radius spheres centered at the peak coordinates of clusters showing significant between-group differences in the ICA-derived network-level comparisons: (1) right hippocampus/parahippocampal gyrus (MNI: +24, −14, −26), and (2) left precentral/postcentral gyri (MNI: −48, −14, +34). For each seed, voxel-wise connectivity maps were computed as Fisher-transformed bivariate correlation coefficients between the seed's BOLD time series and the time series of every other voxel in the brain. These whole-brain maps served as the target voxel-wise connectivity space. The resulting maps were then entered into second-level GLMs to compare connectivity strength between CAC groups, using the same covariate sets (age, sex, and, where applicable, white matter hyperintensity volumes) and correction procedures described for the ICA analyses. Results were visualized as statistical parametric maps thresholded at voxel-level $p < 0.001$ (uncorrected) and cluster-level $p$-FDR $< 0.05$.

To examine connectivity at the network level, we extracted timeseries from each of the 17 ICA-derived networks. For each participant, we then computed functional network connectivity as Fisher-transformed Pearson correlations between every pair of network timeseries, resulting in a $17 \times 17$ connectivity matrix. Finally, we tested for between-group differences in network-to-network connectivity using general linear models, with false discovery rate correction applied across all network pairs to account for multiple comparisons.

### Post-hoc region-of-interest analyses

For hypothesis-driven interrogation of specific circuits, regions of interest (ROIs) were defined as: (a) the peak clusters from ICA analyses, and (b) nodes of canonical resting-state networks from the CONN toolbox atlas, including sensorimotor, salience, frontoparietal, language, dorsal attention, visual, and default mode networks. In addition, we included ROIs from the Harvard-Oxford atlas and 36 HPC-ICA networks to ensure comprehensive coverage.

To compensate for transient magnetization effects at the beginning of each run, individual scans were weighted by a step function convolved with an SPM canonical hemodynamic response function and rectified. For each participant, we then computed bivariate correlations between the BOLD timeseries of all ROI pairs. These correlation coefficients were Fisher-transformed to improve normality and entered second-level analyses. This approach provided finer spatial resolution than network-level analysis while maintaining interpretability within established functional systems.

At the group level, we estimated separate general linear models for each connection, with first-level connectivity measures as dependent variables and groups or subject-level identifiers as independent variables. Connection-level hypotheses were evaluated using multivariate parametric statistics with random effects across subjects and sample covariance estimation across multiple measurements.

To identify broader patterns of network interaction, we performed functional network connectivity analyses using a complete-linkage hierarchical clustering procedure based on ROI-to-ROI anatomical proximity and functional similarity metrics. Inferences were made at the cluster level using parametric statistics within and between pairs of networks. Results were thresholded using a combination of a $p < 0.05$ connection-level threshold and a familywise corrected $p$-FDR $< 0.05$ cluster-level threshold.

### Functional connectivity analysis

ICA component labeling was performed as follows: Each independent component was labeled based on maximum spatial correlation with a set of canonical resting-state network templates (CONN toolbox networks). Components with correlation $r > 0.35$ to multiple template networks (e.g., IC5 correlated with both salience and frontoparietal networks) were assigned the label of the highest correlation but are noted as "overlapping" in Supplementary Fig. 4. Components with identical labels (e.g., two components both matching the visual network) were not combined; they were retained as separate components representing potentially distinct functional subdivisions (e.g., medial vs. lateral visual cortex). All labeled components were visually confirmed by two independent raters (S.M., J.D.M.) with >90% agreement; discrepancies were resolved by consensus.

### Arterial spin labeling

Multi-post-labeling delay (PLD) vessel-encoded pseudo-continuous arterial spin labeling (VEPCASL) was performed to quantify cerebral blood flow (CBF) and enable vessel-territory resolution (left/right internal carotid and vertebrobasilar contributions). For the primary analyses, we report the combined CBF, defined as the sum across all decoded vessel territories. Imaging parameters were as follows: TR 4600 ms, TE 14 ms, flip angle 90°, field of view (read) 200 mm, voxel size $3.1 \times 3.1 \times 5.0$ mm, bandwidth 2004 Hz/Px, and PLDs of 250, 500, 750, 1000, 1250, and 1500 ms (TA 6:18). Because of sequential slice acquisition, the effective PLD for a given slice equals the nominal PLD plus the slice-timing offset; for the central slice this adds ~0.54 s ($12 \times 45.2$ ms), giving central-slice effective PLDs of approximately 0.79, 1.04, 1.29, 1.54, 1.79, and 2.04 s. Slice-timing was explicitly modeled during quantification, so voxelwise fitting used the appropriate effective PLD for each slice. Preprocessing used FSL (v6) and OXASL/BASIL and included reorientation, motion correction using MCFLIRT, tissue segmentation using FSL_ANAT, voxelwise calibration against the calibration image (M0) with standard assumptions (blood–brain partition coefficient $\lambda = 0.9$ mL/g and T1, blood = 1.65 s), and Bayesian multi-PLD fitting in BASIL to derive quantitative CBF (mL/100 g/min). The OXASL pipeline generated CBF maps for the four major brain-supplying arteries[56].

Each VEPCASL run underwent automated motion assessment using MCFLIRT; runs with estimated motion >2 mm translation or >1° rotation were excluded ($n = 3$). Calibration (M0) images were inspected for artifacts. Voxel-wise CBF maps were visually screened for coverage failures, susceptibility artifacts, and incomplete vessel encoding ($n = 6$ excluded).

Whole-brain mean CBF values were additionally examined for outliers; values < 20 or >80 mL/100 g/min triggered manual review of raw data and quantification parameters ($n = 2$ corrected, $n = 1$ excluded).

### Arterial spin labeling processing

Three-dimensional time-of-flight angiography was used to localize the right and left internal carotid arteries and the right and left vertebral arteries, which were tagged separately using an eight-cycle paired encoding scheme. Structural preprocessing was performed using fsl_anat on the T1-weighted image (bias-field correction, brain extraction, and tissue segmentation), generating the structural-to-Montreal Neurological Institute (MNI) non-linear transformation used for subsequent registration steps. VEPCASL data were processed using OXASL (Python) v0.2.2 with the vessel-encoded plugin oxasl_ve v0.3.1, which performs vessel decoding prior to kinetic modeling. ASL images were registered using outputs from fsl_anat, perfusion-weighted images were generated, and voxel-wise perfusion was computed using the supplied M0 image with the Bayesian Inference for Arterial Spin Labeling (BASIL) toolbox[60]. Perfusion modeling incorporated six PLDs (0.25–1.50 s), a fixed bolus duration ($\tau = 1.4$ s), and a per-slice acquisition time $\Delta$t_slice = 45.2 ms with slice timing accounted for in the model fit. CBF was estimated using a BASIL two-compartment model, including tissue and explicit macrovascular compartments with arterial transit time inferred; no dispersion model was applied. BASIL options included partial-volume correction, adaptive spatial smoothing of perfusion images, and motion correction using MCFLIRT. Voxelwise calibration used the M0 image with an inversion efficiency of 0.85 and T1, blood = 1.65 s at 3T.

Region-based statistics were generated using Harvard–Oxford atlas regions transformed from MNI to each participant's native ASL space using fsl_anat warps. Only voxels with ≥ 50% gray matter probability were retained, and a minimum threshold of 10 contiguous voxels was required to ensure reliable regional estimates. Regions not meeting this criterion were coded as missing; this predominantly affected small subcortical structures (e.g., amygdala, thalamic sub-regions, accumbens) due to the relatively coarse ASL resolution and partial volume effects. Missingness was balanced between CAC groups and was not associated with age, sex, or CAC score (all $p > 0.20$), suggesting no systematic bias. ROIs were masked using "pure" gray- and white-matter masks. Alzheimer's disease-related regions, including the posterior cingulate, precuneus, and temporo-limbic cortices, were selected for their discriminatory value in mild Alzheimer's disease (Supplementary Tables 3 and 4)[61]. Sample processing code can be requested from the authors.

### Statistical analysis

Analyses were performed using R version 4.3.2. Group differences in cognitive, serum, and brain volumes outcomes were assessed using ANCOVA, adjusting for age, sex, education, and time between CT-MRI assessments. Blood flow analyses were corrected for age and sex. Non-normally distributed variables were log-transformed or analyzed using Mann–Whitney U tests. *P*-values were corrected for multiple comparisons using the Benjamini–Hochberg procedure ($p$-FDR < 0.05). Functional connectivity analyses used GLMs, with voxel-wise corrections applied via random field theory ($p$-FDR < 0.05). Effect sizes are reported as eta-squared ($h^2$), reflecting the magnitude of the seed-to-voxel functional connectivity between-group difference. Post hoc ROI-to-ROI functional connectivity was assessed via F-tests for connections.

## Data availability

The datasets generated and analyzed during the current study are not publicly available due to ethical and privacy restrictions associated with human participant data, but are available from the corresponding author on reasonable request and subject to institutional and Lifelines data access policies.

Received: 15 December 2025; Accepted: 22 April 2026;
Published online: 01 June 2026

## References

1. Libby, P. PART IV *PREVENTIVE CARDIOLOGY 24 The Vascular Biology of Atherosclerosis*. *Braunwald's Heart Disease*, *2 Vol Set*. https://doi.org/10.1016/B978-0-323-72219-3.00024-4 (Elsevier Inc., 2023).
2. De La Torre, J. C. Cardiovascular risk factors promote brain hypoperfusion leading to cognitive decline and dementia. *Cardiovasc. Psychiatry Neurol*. **2012**, 367516 (2012).
3. de la Torre, J. C. et al. An integrated view on vascular dysfunction in Alzheimer's Disease. *Acta Neuropathol.* **26**, 111184 (2020).
4. Budoff, M. J. et al. Ten-year association of coronary artery calcium with atherosclerotic cardiovascular disease (ASCVD) events: the multi-ethnic study of atherosclerosis (MESA). *Eur. Heart J.* **39**, 2401–2408 (2018).
5. Haq, A. et al. Coronary artery calcium and the risk of cardiovascular events and mortality in younger adults: a meta-analysis. *Eur. J. Prev. Cardiol*. https://doi.org/10.1093/eurjpc/zwad399 (2023).
6. Bos, D. et al. Atherosclerotic calcification is related to a higher risk of dementia and cognitive decline. *Alzheimer's. Dement.* **11**, 639–647.e1 (2015).
7. Kuller, L. H. et al. Subclinical atherosclerosis, cardiac and kidney function, heart failure, and dementia in the very elderly. *J. Am. Heart Assoc*. **6**, e005353 (2017).
8. Kuller, L. H. et al. Subclinical Cardiovascular Disease and Death, Dementia, and Coronary Heart Disease in Patients 80þ Years. *J. Am. Coll. Cardiol*. **67**, 1013–1022 (2016).
9. Fujiyoshi, A. et al. Coronary artery calcium and risk of dementia in MESA (Multi-Ethnic Study of Atherosclerosis). *Circ. Cardiovasc. Imaging* **10**, e005349 (2017).
10. Mézquita, A. J. V. et al. Clinical quantitative coronary artery stenosis and coronary atherosclerosis imaging: a Consensus Statement from the Quantitative Cardiovascular Imaging Study Group. *Nat. Rev. Cardiol.* https://doi.org/10.1038/s41569-023-00880-4 (2023).
11. Golub, I. S. et al. Major global coronary artery calcium guidelines. *JACC Cardiovasc. Imaging* **16**, 98–117 (2023).
12. Bos, D. et al. Atherosclerotic calcification relates to cognitive function and to brain changes on magnetic resonance imaging. *Alzheimer's Dement.* **8**, S104-11 (2012).
13. Suemoto, C. K., Bittencourt, M. S., Santos, I. S., Benseñor, I. M. & Lotufo, P. A. Coronary artery calcification and cognitive function: cross-sectional results from the ELSA-Brasil study. *Int. J. Geriatr. Psychiatry* **32**, e188–e194 (2017).
14. Reis, J. P. et al. Subclinical atherosclerotic calcification and cognitive functioning inmiddle-aged adults: the CARDIA study. *Atherosclerosis* **231**, 72–77 (2013).
15. Gatto, N. M. et al. Subclinical atherosclerosis is weakly associated with lower cognitive function in healthy hyperhomocysteinemic adults without clinical cardiovascular disease. *Int. J. Geriatr. Psychiatry* **24**, 390–399 (2009).
16. Lee, J. S. et al. Coronary artery calcium is associated with cortical thinning in cognitively normal individuals. *Sci. Rep*. **6**, 34722 (2016).
17. Jin, H. et al. Is coronary artery calcium an independent risk factor for white matter hyperintensity? *BMC Neurol*. **23**, 313 (2023).
18. Kneihsl, M. et al. Cerebral white matter hyperintensities indicate severity and progression of coronary artery calcification. *Sci. Rep*. **14**, 4664 (2024).
19. Khan, M. M. H. et al. The association between coronary artery calcification and subclinical cerebrovascular diseases in men: an observational study. *J. Atheroscler. Thromb.* **27**, 995–1009 (2020).
20. Kim, B. J. et al. Advanced coronary artery calcification and cerebral small vessel diseases in the healthy elderly. *Circ. J.* **75**, 451–456 (2011).

21. Lin, S. et al. Altered functional brain networks in coronary heart disease: independent component analysis and graph theoretical analysis. *Brain Struct. Funct.* **229**, 133–142 (2024).
22. Sun, Z. et al. Decreased regional spontaneous brain activity and cognitive dysfunction in patients with coronary heart disease: a resting-state functional MRI study. *Acad. Radiol.* **30**, 1081–1091 (2023).
23. Veldsman, M. et al. Cerebrovascular risk factors impact frontoparietal network integrity and executive function in healthy ageing. *Nat. Commun*. **11**, 4340 (2020).
24. Jia, J. et al. Biomarker changes during 20 years preceding Alzheimer's disease. *N. Engl. J. Med.* **390**, 712–722 (2024).
25. Ossenkoppele, R. et al. Amyloid and tau PET-positive cognitively unimpaired individuals are at high risk for future cognitive decline. *Nat. Med*. **28**, 2381–2387 (2022).
26. Milà-Alomà, M. et al. Amyloid beta, tau, synaptic, neurodegeneration, and glial biomarkers in the preclinical stage of the Alzheimer's continuum. *Alzheimer's Dement.* **16**, 1358–1371 (2020).
27. Teunissen, C. E. et al. Blood-based biomarkers for Alzheimer's disease: towards clinical implementation. *Lancet Neurol.* **21**, 66–77 (2022).
28. De Meyer, S. et al. Longitudinal associations of serum biomarkers with early cognitive, amyloid and grey matter changes. *Brain* **147**, 936–948 (2024).
29. Calsolaro, V. & Edison, P. Neuroinflammation in Alzheimer's disease: current evidence and future *directions*. *Alzheimer's Dement.* **12**, 719–732 (2016).
30. Kinney, J. W. et al. Inflammation as a central mechanism in Alzheimer's disease. *Alzheimer's Dement. Transl. Res. Clin. Interv.* **4**, 575–590 (2018).
31. Avula, V. et al. Inflammatory markers and calcification of coronary arteries, aorta and cardiac valves: findings from the atherosclerosis risk in communities study. *Am. J. Prev. Cardiol.* **21**, 100946 (2025).
32. Raaz-Schrauder, D. et al. Association of systemic inflammation markers with the presence and extent of coronary artery calcification. *Cytokine* **57**, 251–257 (2012).
33. Hamirani, Y. S. et al. Markers of inflammation and coronary artery calcification: a systematic review. *Atherosclerosis* **201**, 1–7 (2008).
34. Jenny, N. S. et al. Associations of inflammatory markers with coronary artery calcification: results from the multi-ethnic study of atherosclerosis. *Atherosclerosis* **209**, 226–229 (2010).
35. Xia, C. et al. Coronary artery calcium and cognitive function in Dutch adults: cross-sectional results of the population-based IMALIFE study. *J. Am. Heart Assoc.* **10**, 1–12 (2021).
36. Polk, S. E. et al. A scoping review of remote and unsupervised digital cognitive assessments in preclinical Alzheimer's disease. *NPJ Digit. Med.* **8**, 266 (2025).
37. Wu, M. et al. In pre-clinical AD small vessel disease is associated with altered hippocampal connectivity and atrophy. *Am. J. Geriatr. Psychiatry* **31**, 112–123 (2023).
38. Liu, R. et al. The altered reconfiguration pattern of brain modular architecture regulates cognitive function in cerebral small vessel disease. *Front. Neurol*. **10**, 324 (2019).
39. Chen, H. et al. The dose-dependent effects of vascular risk factors on dynamic compensatory neural processes in mild cognitive impairment. *Front. Aging Neurosci*. **10**, 131 (2018).
40. Marcolini, S. et al. Effects of interventions on cerebral perfusion in the Alzheimer's disease spectrum: a systematic review. *Ageing Res. Rev.* **79**, 101661 (2022).
41. Yang, H. S. et al. Plasma VEGFA and PGF impact longitudinal tau and cognition in preclinical Alzheimer's disease. *Brain Neurosci. J.* **147**, 2158–2168 (2024).
42. Ashton, N. J. et al. Diagnostic accuracy of a plasma phosphorylated Tau 217 immunoassay for Alzheimer disease pathology. *JAMA Neurol.* **81**, 255 (2024).
43. Xia, C. et al. Early imaging biomarkers of lung cancer, COPD and coronary artery disease in the general population: rationale and design of the ImaLife (Imaging in Lifelines) study. *Eur. J. Epidemiol.* **35**, 75–86 (2020).
44. Agatston, A. S. et al. Quantification of Coronary Artery Calcium Using Ultrafast Computed Tomography. *JACC* **15**, 827–832 (1990).
45. Folstein, M. F., Folstein, S. E. & McHugh, P. R. 'Mini-mental state'. A practical method for grading the cognitive state of patients for the clinician. *J. Psychiatr. Res.* **12**, 189–198 (1975).
46. Brand, N. & Jolles, J. Learning and retrieval rate of words presented auditorily and visually. *J. Gen. Psychol.* **112**, 201–210 (1985).
47. Rey, A. L'examen clinique en psychologie (Presses Universitaires de France, 1964).
48. Reitan, R. M. Validity of the trail making test as an indicator of organic brain damage. *Percept. Mot. Skills* **8**, 271–276 (1958).
49. Tiffin, J. & Asher, E. J. The Purdue pegboard; norms and studies of reliability and validity. *J. Appl. Psychol.* **32**, 234–247 (1948).
50. Van Der Elst, W., Van Boxtel, M., Van Breukelen, G. & Jolles, J. The letter digit substitution test: normative data for 1,858 healthy participants aged 24-81 from the Maastricht Aging Study (MAAS): Influence of age, education, and sex. *J. Clin. Exp. Neuropsychol.* **28**, 998–1009 (2006).
51. Lindeboom, J., Schmand, B., Tulner, L., Walstra, G. & Jonker, C. Visual association test to detect early dementia of the Alzheimer type. *J. Neurol. Neurosurg. Psychiatry* **73**, 126–133 (2002).
52. Wechsler, D. *Wechsler Adult Intelligence Scale—Third Edition* (APA PsycTests, 1997).
53. Stroop, J. R. Studies of interference in serial verbal reactions. *J. Exp. Psychol.* **18**, 643–662 (1935).
54. Lezak, M. *Neuropsychological Assessment* (Oxford University Press, 1995).
55. Hoogendam, Y. Y., Hofman, A., Van Der Geest, J. N., Van Der Lugt, A. & Ikram, M. A. Patterns of cognitive function in aging: the Rotterdam Study. *Eur. J. Epidemiol.* **29**, 133–140 (2014).
56. Okell, T. W., Chappell, M. A., Kelly, M. E. & Jezzard, P. Cerebral blood flow quantification using vessel-encoded arterial spin labeling. *J. Cereb. Blood Flow. Metab.* **33**, 1716–1724 (2013).
57. Iorio, M. et al. White matter hyperintensities segmentation: a new semi-automated method. *Front. Aging Neurosci*. **5**, 76 (2013).
58. Whitfield-Gabrieli, S. & Nieto-Castanon, A. Conn: a functional connectivity toolbox for correlated and anticorrelated brain networks. *Brain Connect.* **2**, 125–141 (2012).
59. Marcolini, S. et al. Small vessel disease burden and functional brain connectivity in mild cognitive impairment. *Cereb. Circ. Cogn. Behav.* **6**, 100192 (2024).
60. Chappell, M. A. et al. BASIL: a toolbox for perfusion quantification using arterial spin labelling. *Imaging Neurosci.* **1**, 1–16 (2023).
61. Rondina, J. M. et al. Selecting the most relevant brain regions to discriminate Alzheimer's disease patients from healthy controls using multiple kernel learning: a comparison across functional and structural imaging modalities and atlases. *NeuroImage Clin.* **17**, 628–641 (2018).


## Acknowledgements

We sincerely thank the volunteers recruited through Lifelines and the Memolife study for their participation. S.M. is supported by an institutional grant, PUSH: Partnership of UMCG - Siemens Healthineers for building the future of Health and by the Joint Programming Initiative Neurodegenerative Diseases (JPND) HEROES project (No.: 733051072). We are also grateful for the support of Neurosearch Antwerp. T.W.O. is supported by a Sir Henry Dale Fellowship jointly funded by the Wellcome Trust and the Royal Society (220204/Z/20/Z). The Oxford Centre for Integrative Neuroimaging was previously supported by core funding from the Wellcome Trust (203139/Z/16/Z) with additional support from the NIHR Oxford Health Biomedical Research Centre (NIHR203316). The views expressed are those of the authors and not necessarily those of the NIHR or the Department of Health and Social Care. For the purpose of open access, the author has applied a

 I.M.W.V. performs contract research or receives consultancy or speaker fees from Nitrase Therapeutics, Roche Diagnostics, Neurogen Biomarking, Quanterix and Olink. All is paid directly to her institution.

## Author contributions

S.M., R.A.J.O.D., R.J.H., and P.P.D.D. conceived and designed the study, developed the methodology and data-collection protocol. S.M. collected and curated the data, together with J.M. and J.C. S.M., J.M., and J.C. performed the statistical analyses and interpreted the results, also with support from the other co-authors. S.M., J.M, and J.C. produced the figures and tables. T.W.O. provided technical support for the arterial spin labeling data acquisition and analysis, C.E.T. and I.M.W.V. for the blood biomarkers analyses. R.V. is the Principal Investigator of the Imalife study, and A.H. provided neuroradiological support. S.M. and J.M. drafted the manuscript. All other co-authors critically revised the manuscript. R.A.J.O.D., R.J.H., and P.P.D.D. supervised the project, secured funding and provided resources. All authors read and approved the final version of the manuscript.

## Competing interests

The authors declare no competing interests.

## Additional information

**Supplementary information** The online version contains supplementary material available at https://doi.org/10.1038/s44400-026-00093-9.

**Correspondence** and requests for materials should be addressed to Sofia Marcolini.